Journal of Colloid and Interface Science 668 (2024) 540–550

Contents lists available at ScienceDirect

Journal of Colloid And Interface Science

journal homepage: www.elsevier.com/locate/jcis

Regular Article

Persistent production of multiple active species with copper doped zinc gallate nanoparticles for light-independent photocatalytic degradation of organic pollutants

Dong-Mei Zhou [a,b,c], Li-Jian Chen [a,b,c,*], Xu Zhao [a,b,c], Li-Xia Yan [a,b,c], Xiu-Ping Yan [a,b,c,d,*]

[a] State Key Laboratory of Food Science and Resources, Jiangnan University, Wuxi 214122, China
[b] International Joint Laboratory on Food Safety, Jiangnan University, Wuxi 214122, China
[c] Institute of Analytical Food Safety, School of Food Science and Technology, Jiangnan University, Wuxi 214122, China
[d] Key Laboratory of Synthetic and Biological Colloids, Ministry of Education, School of Chemical and Material Engineering, Jiangnan University, Wuxi 214122, China

HIGHLIGHTS

- Nanosized $ZnGa_2O_4$:Cu was designed for continuously degrading pollutants.
- The doping of Cu(II) highly increased the persistent production and availability of active species.
- •H radicals were identified as the main active species.
- A possible mechanism for the persistent degradation of dyes was proposed.

GRAPHICAL ABSTRACT

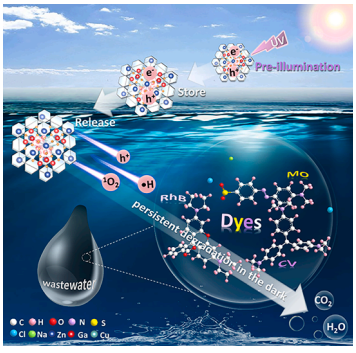

ARTICLE INFO

Keywords:
Copper doped zinc gallate
Active species
Persistent photocatalytic degradation
Organic dyes

ABSTRACT

Photocatalysis is considered as an environmentally friendly and sustainable method as it can produce active species to degrade pollutants. However, its applications are hindered by the turbidity of pollutants and the requirements for continuous or repeated in situ irradiation. To avoid the need for continuous in situ irradiation in the photocatalytic process, herein we report the doping of Cu(II) ions into zinc gallate ($ZnGa_2O_4$) as traps to capture photo-generated electrons. In this way, long lifetime charge release and separation were effectively achieved for the persistent degradation of organic dyes in wastewater. The Cu(II) doped $ZnGa_2O_4$ (ZGC) nanoparticles with a small size about 7.7 nm synthesized via a hydrothermal method exhibited a persistent photocatalytic activity with continuous production of reactive oxygen species for at least 96 h without in situ irradiation due to its unique electronic structure and carrier transport path, and enabled to degrade 82.2 % of rhodamine B in 1 h. Further investigation revealed that the doped Cu(II) ions occupied the octahedral sites of ZGC and highly increased the persistent production and availability of active species for the persistent degradation of organic dyes under pre-illuminated conditions.

* Corresponding author at: State Key Laboratory of Food Science and Resources, Jiangnan University, Wuxi 214122, China.
E-mail addresses: chenlijian123@jiangnan.edu.cn (L.-J. Chen), xpyan@jiangnan.edu.cn (X.-P. Yan).

https://doi.org/10.1016/j.jcis.2024.04.135
Received 5 February 2024; Received in revised form 6 April 2024; Accepted 19 April 2024
Available online 20 April 2024

1. Introduction

Organic dyes are one of the main sources of water pollution, posing serious threats to the food chain and water bodies due to their huge demand from various fields, including paper mill, textile, plastic, food, and pharmaceutical industries [1,2]. To reduce the impact of organic dye wastewater, a series of remedial methods have been utilized, such as photocatalysis, adsorption, and biodegradation [3]. Among these methods, photocatalysis is an environmentally friendly and economical approach with no secondary pollutants since it can generate active species including reactive oxygen species (ROS) to effectively eliminate organic pollutants [4,5]. In general, semiconductor catalysts in photocatalytic reactions undergo three consecutive processes including the generation of photo-electrons (e^-) and holes (h^+), the migration of these e^- and h^+ to the surface of the material, and redox reactions on the surface, leading to the formation of active species [6,7]. According to the above processes, traditional semiconductor catalysis cannot be performed in the absence of light sources. Thus, the key limitation of traditional semiconductor catalysts is the poor light utilization efficiency in the dark condition or the solution with a low light penetration [8]. To address this limitation, it is significant to design novel materials for persistent photocatalysis of organic pollutants in the absence of light.

Long persistent photocatalysts can avoid the dependence on in situ excitation in conventional photocatalysis and prolong the operation of photocatalysis in the dark due to their unique electron-storage component [9,10]. Typical long persistent photocatalytic processes can be described as the e^- generation after irradiation, the transfer of e^- into the conduction bands as well as the corresponding h^+ formation in the valence bands of materials. The e^- and h^+ can be stored in the traps. After irradiation stops, the e^- and h^+ on the traps can slightly release and migrate to the surface of materials for oxidation–reduction reactions [10]. It is very important to promote the migration efficiency of e^- and h^+ to the surface of catalysts for persistent photocatalytic reaction after removing the excitation source. Besides, the inherent excellent photocatalytic activity also plays a key role in long persistent photocatalysis. Therefore, the first step is to select a suitable catalyst matrix.

Alkaline earth gallates (AB_2O_4) exhibit excellent photocatalytic performance [9]. P-block metal oxides with d^{10} configuration have great potential as photocatalysts [11]. Zinc gallate ($ZnGa_2O_4$, ZGO) is a ternary metal-oxide-based spinel with two d^{10} cations, a wide bandgap, and good chemical and thermal stability [12,13]. Due to its unique performance, ZGO has been widely utilized in the field of photocatalysis for hydrogen production, CO_2 reduction, and antibiotics degradation [14–16]. Generally, Zn ions locate in the tetrahedron while Ga ions in the octahedron of the crystalline structure of ZGO. The valence band and conduction band are respectively composed of the O 2p atomic orbitals of lattice O^{2-} ions and the Ga 3d atomic orbitals of lattice Ga^{3+} ions in GaO_6 octahedron [17]. This unique electronic structure makes ZGO a prospective and ideal catalytic matrix for potential persistent photocatalytic application, especially since it is not only a luminescent material but also an electron storage material [7,18]. However, the low efficiency for the charge separation and active species generation of ZGO spinels limits further wide applications.

Several approaches are available to improve the efficiency for the charge separation and active species generation of host materials. Transition metal-doping is an essential way to promote the activity of photocatalytic degradation as it can introduce new levels or adjust energy band structure to inhibit the rapid combination of photo-generated carriers [12]. Han et al. [19] reported that Cu(II)-doped PCN 224 significantly increased the production of ROS due to the effective trapping of e^- by Cu(II) doping, which enhanced the separation of photo-generated charge carriers. Gong et al. [20] prepared Cu(II)-doped Zn_2GeO_4 persistent luminescence nanorods with excellent ability for persistent ROS production. The introduction of Cu(II) ions acted as traps to store photo-generated carriers, endowing the Cu(II)-doped Zn_2GeO_4 nanorods with persistent photocatalytic properties even after the excitation stopped. However, Zn_2GeO_4 nanorods are unsuitable for photocatalytic application due to their instability in acidic environment [7,20]. Furthermore, although numerous studies have been reported on round-the-clock photocatalysis, most of the catalysts are big-sized materials, such as micron-size [21]. It was found that the small-sized semiconductor materials (<10 nm) gave higher photocatalytic activity than big-sized materials (e.g. μm) as their short migration path greatly inhibited the recombination rate of e^- and h^+ pairs [22].

Herein, we report the synthesis of Cu(II)-doped ZGO nanoparticles (ZGC) via a hydrothermal method for efficient persistent photocatalysis of three organic dyes in the absence of in-situ irradiation light sources. ZGO was selected as the matrix material due to its unique electronic structure [7,18]. Cu(II) was introduced to ZGO as the trap center to store photo-generated charge carriers upon light excitation. Thus, the stored carriers could release for a period, and continuously migrate to the surface of ZGC to initiate redox reactions for the degradation of organic dyes after the stopping of light excitation. The active species including hydrogen radicals (•H), superoxide radicals ($\bullet O_2^-$), singlet oxygen ($^1O_2$) and h^+ after pre-illumination were found, and the persistent photocatalytic mechanism of ZGC was also proposed.

2. Experimental

2.1. Chemicals and materials

$Zn(NO_3)_2{\cdot}6H_2O$ (99.99 %), $Ga(NO_3)_3{\cdot}xH_2O$ (99.99 %), ammonium hydroxide ($NH_3{\cdot}H_2O$, 25 %-28 %), cetyltrimethyl ammonium bromide (CTAB, 99 %), isopropyl alcohol (IPA, 99.7 %), benzoquinone (BQ, 98 %), ammonium oxalate (AO, 99.5 %), L-histidine (L-His, 99 %), ethanol (99.7%) and crystal violet (CV, 90 %) were purchased from Sinopharm Chemical Reagent Co., Ltd (Shanghai, China). Ultrapure water was purchased from Wahaha Group Co. (Hangzhou, China). $Cu(NO_3)_2{\cdot}3H_2O$ (99 %), 2′,7′-dichlorodihydrofluorescein diacetate (DCFH-DA, 97 %), 5,5-diamethyl-1-pyrroline *N*-oxide (DMPO, 98 %), 2,2,6,6-tetramethylpiperidine (TEMP, 98 %), 2,2,6,6-tetramethylpiperidine-1-oxyl (TEMPO, 98 %), methylene blue (MB, 96 %), methyl orange (MO, 96 %), were purchased from Aladdin (Shanghai, China). Rhodamine B (RhB, 96 %) was purchased from J&K Scientific (Shanghai, China).

2.2. Apparatus

X-ray diffraction (XRD) spectra were recorded on a D2 PHASER diffractometer (Bruker AXS, Germany). Electron paramagnetic resonance spectroscopy (EPR) experiments were performed on an EMXplus-10/12 spectrometer (Bruker, Germany). Transmission electron microscopy (TEM) images were obtained on a JEM-2100 transmission electron microscope (JEOL, Japan). The DigitalMicrograph software was used to analyse the fast Fourier transform (FFT) diffraction pattern, inverse fast Fourier transform (IFFT) patterns, and lattice spacing of nanomaterials from high-resolution TEM (HRTEM) images. Nitrogen adsorption experiments were performed on Autosorb-iQ (Quantachrome, USA) using N_2 adsorption at 77 K. X-ray photoelectron spectroscopy (XPS) experiments were carried out on an Axis supra with monochromatized Al Ka radiation (hv = 1486.6 eV) as X-ray source (Kratos, UK). All spectra were calibrated by the C 1 s peak at 284.8 eV. Zeta potentials were acquired on a Nano Zetasizer (ZEN 3700, Malvern Instruments, Manchester, UK). Photoluminescence (PL) spectra were collected on a F-7000 fluorescence spectrophotometer (Hitachi, Japan). UV–vis diffuse reflectance spectra were acquired on a UV-3600i Plus spectrophotometer (Shimadzu, Japan). The fluorescence of ROS indicator was measured on a Synergy H1 microplate reader (Bio Tek, America). UV–vis absorption spectra were recorded on a UV-3600 PLUS spectrophotometer (Shimadzu, Japan). Time-resolved fluorescence decay spectra were obtained on FLS1000 (Edinburgh, UK). Raman spectra were collected on DXRxi with a 532 nm excitation source (Thermo, USA).

2.3. Synthesis of ZGC and ZGO nanoparticles

ZGC and ZGO nanoparticles were synthesized via a facile hydrothermal process [20,23]. In a typical synthesis of ZGC, the solutions of zinc nitrate (2 mL, 0.5 mol/L), gallium nitrate (4 mL, 0.5 mol/L), and copper nitrate (63 μL 0.08 mol/L) were thoroughly mixed. CTAB (2 mg) was added to the mixed solution and the mixed solution was ultrasonicated at room temperature for 5 min. The reaction solution was adjusted to pH 8.0 with ammonium hydroxide and stirred constantly for 1 h, then the homogenous solution was transferred into a 25 mL Teflon-liner autoclave and heated at 220 °C for 24 h. After the reaction mixture was cooled to room temperature, the resulting ZGC was collected by centrifugation, washed with 0.01 M HCl and ethanol for several times, and dried in vacuum at 60 °C for further persistent photocatalytic application. ZGO was synthesized by the same procedure except that no solution of copper nitrate was added.

2.4. Measurement of ROS using DCFH indicator

The ROS produced by the typical ZGC nanoparticles was determined by a ROS assay kit. Firstly, DCFH-DA was converted to 2′,7′-dichlorodihydrofluorescein (DCFH) in the ROS assay kit. In brief, DCFH-DA (0.5 mL, 1 mmol/L) in ethanol was added into NaOH solution (2 mL, 10 mmol/L) and the mixture was reacted at room temperature for 30 min. The above mixture was neutralized with PBS buffer (10 mL, 25 mmol/L, pH 7.4) and stored at −20 °C in the dark for further use [24]. Subsequently, ZGC nanoparticles were illuminated with a UV lamp (6 W, 254 nm) for 60 min and mixed with DCFH (40 μmol/L) immediately. The mixture was allowed to react in the dark for 30 min. After that, the supernatant was harvested by centrifugation, and the fluorescence (FL) intensity at 525 nm was recorded on a Synergy H1 microplate reader with an excitation wavelength of 488 nm.

2.5. Test of persistent photocatalytic activity

The persistent photocatalytic activity of the as-synthesized photocatalysts ZGO and ZGC was evaluated by monitoring the UV–vis absorption of RhB, MB, MO, CV, and RhB/MB/MO/CV mixture solutions. In a typical persistent photocatalytic test, 0.3 g photocatalyst powders were firstly irradiated by a UV lamp (254 nm, 20 μW cm^{-2}) for 60 min. After UV light irradiation, the pre-irradiated photocatalyst powders were put into dye solutions (10 mg/L, 30 mL) for degradation in the dark. The final concentration of each dye in the mixed dye solution was 10 mg/L while that of the as-prepared ZGC or ZGO was 10 g/L. The parallel experiments for the un-irradiated ZGC or ZGO were conducted as reference as well. A certain volume of the suspension was collected at predetermined times to measure the absorbance of RhB, MB, MO, CV, and mixture solutions after the centrifugation removal of the photocatalyst. The efficiency of degradation was calculated as C/C_0, where C_0 is the initial concentration of each dye, and C is the remaining concentration of each dye after persistent photocatalytic reaction.

3. Results and discussion

3.1. Optimization of ZGC preparation and characterization of ZGO and ZGC

The preparation of ZGC for the persistent degradation of organic dyes is illustrated in Scheme 1. To obtain the ZGC with the best persistent photocatalytic property, the Cu(II) doping ratio and reaction conditions were optimized. As the ROS generation ability plays a key role in the persistent photocatalytic process, the ROS produced by ZGC was measured using DCFH as a fluorescent probe. DCFH can be oxidized by ROS to 2′,7′-dichlorofluorescein (DCF) which gives strong fluorescence. The enhanced fluorescence intensity has a close relation to the concentration of ROS. As shown in Fig. S1, all of the Cu(II) doping ratio, reaction pH, time, and temperature had effect on the ROS production of ZGC. The highest fluorescence intensity appeared at the Cu(II) doping ratio of 0.25 % (Fig. S1a), the reaction pH 8.0 (Fig. S1b), the hydrothermal time of 24 h (Fig. S1c) and the hydrothermal temperature of 220 °C (Fig. S1d).

The PL spectra of the as-prepared ZGC under different synthesis conditions were measured to reveal the effect of synthesis conditions on the separation of photogenerated charge carriers. According to the principle of PL peak production, the separation of photo-generated e^--h^+ pairs can be directly reflected in the PL spectrum. That is, the weaker the PL intensity, the lower the recombination rate of photogenic carriers [25]. The PL intensity of the prepared ZGC decreased sharply as the Cu (II) doping ratio increased (Fig. S2a), while the lowest PL intensity appeared at the pH of 8.0 and the hydrothermal temperature of 220 °C

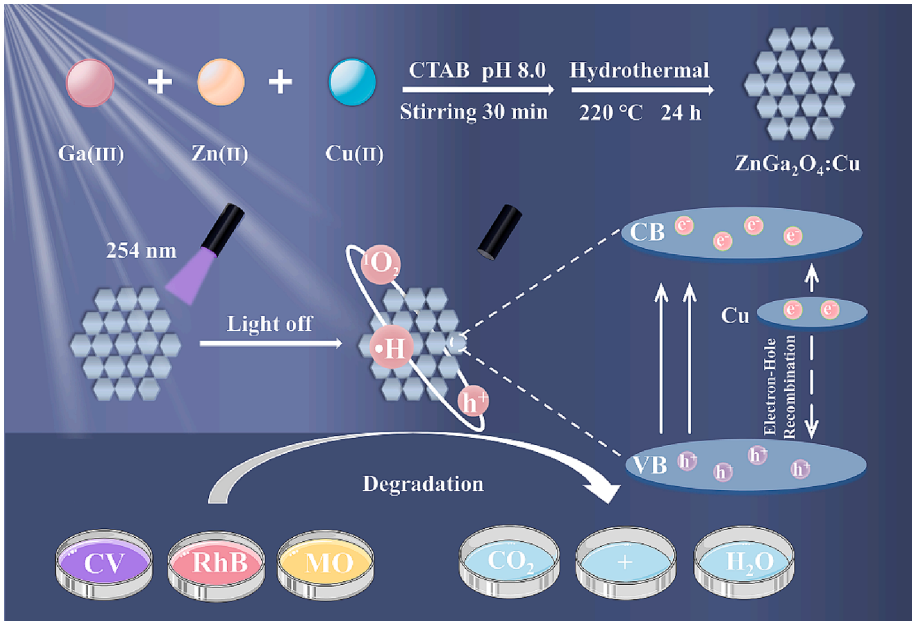

Scheme 1. Illustration for the preparation of ZGC for the persistent photocatalytic degradation of organic dyes.

(Fig. S2b and 2c). However, the hydrothermal time showed little effect on the PL intensity (Fig. S2d). The above results indicate the significant effect of Cu(II) doping on the separation of photogenerated charge carriers.

The diffraction peaks slightly shifted to higher angles as the Cu(II) doping ratio increased (Fig. S3a and S3b). However, the phase of ZnO (JCPDS card no. 36–1451) was detected at the hydrothermal temperature of 220 °C (Fig. S3c). It is possible that Zn^{2+} was not fully involved in the formation of ZGC under high hydrothermal temperature, thus excess Zn^{2+} can be dissolved by the formation of soluble ammonium complexes, generating ZnO impurity [26]. To gain pure ZGC nanoparticles, ZnO impurity was removed through a washing step with HCl solution, as confirmed by HRTEM (Fig. 1a–c *vs.* Fig. S4a–c).

The crystalline structures show good evolution trends under different conditions except pH 10.0 and a hydrothermal time of 48 h which led to the destruction of the crystal phase of ZGC (Fig. S3). Based on the above results, the optimal conditions (Cu(II) doping ratio of 0.25 %, pH 8.0, hydrothermal time of 24 h, and hydrothermal temperature of 220 °C) were selected for the preparation of ZGC.

The crystal phases of HCl-treated ZGC and ZGO were identified by XRD spectrometry. As shown in Fig. 1f and g, all diffraction patterns were well matched to the spinel structure of ZGO (JCPDS card no. 38–1240). Compared with ZGO, the diffraction peaks of ZGC showed very slight diffraction shift to higher angles, probably due to the

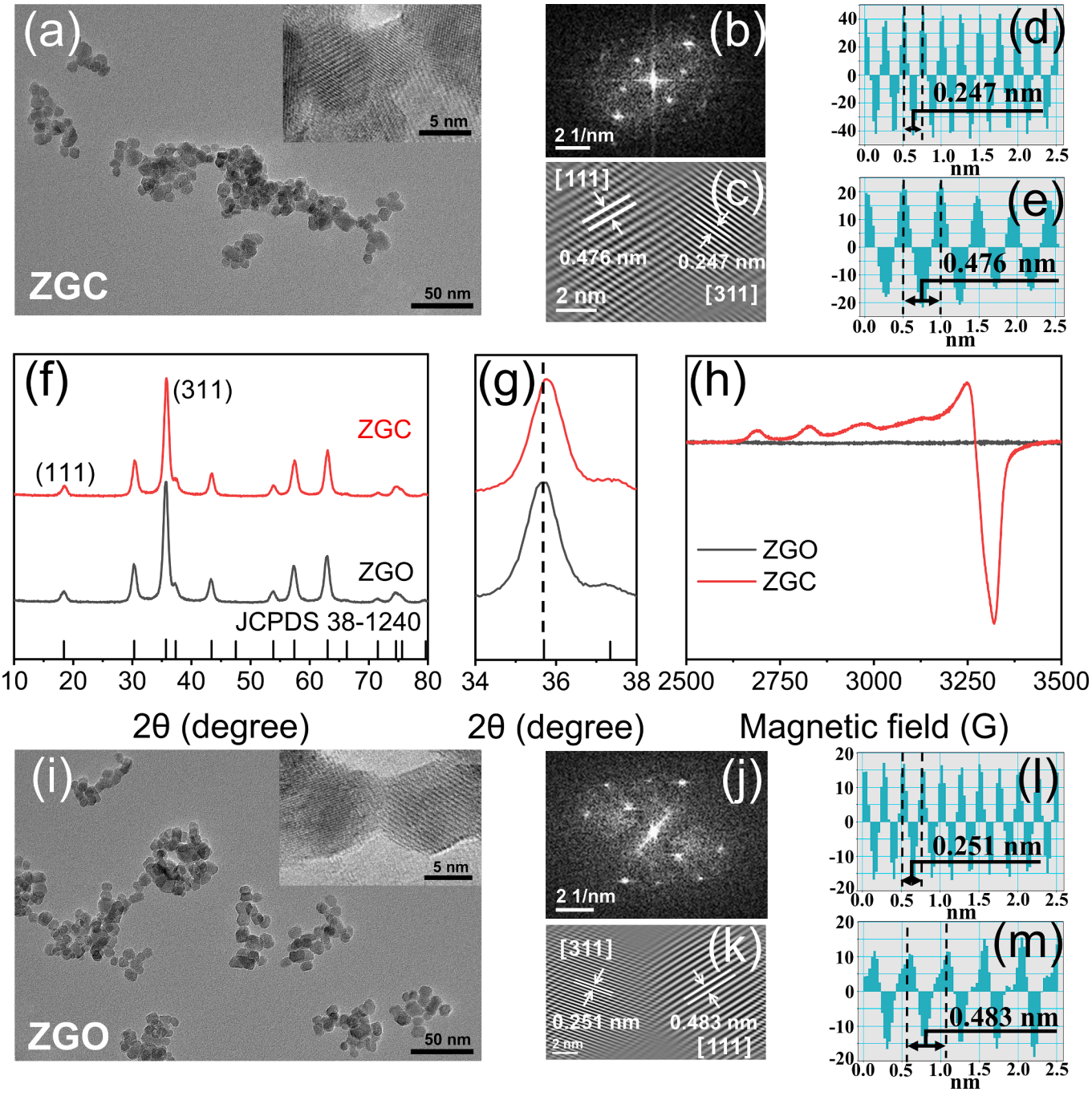

Fig. 1. Characterization of the as-prepared ZGC and ZGO. (a, b, c, d, e) TEM image (inset, HRTEM image), FFT pattern, IFFT pattern and the corresponding lattice spacing profile of ZGC; (f, g) XRD patterns; (h) EPR patterns; (i, j, k, l, m) TEM image (inset, HRTEM image), FFT pattern, IFFT pattern and the corresponding lattice spacing profile of ZGO.

compromise of lattice shrinking with Cu doping [27]. To further verify the Cu doping, EPR spectra were collected (Fig. 1h). Cu(II) ions are paramagnetic and can cause the occurrence of anisotropic EPR spectra [28,29]. The EPR spectrum of ZGC exhibited characteristic Cu(II) signals with an axial g-tensor and a four-line hyperfine coupling pattern due to the Cu nuclear spin 3/2 [30]. In addition, a five-line spectrum was observed, indicating the simultaneous occurrence of apparently compressed and elongated octahedral complexes [28]. These results indicate that the Cu(II) was doped into the ZGO host lattices and situated on the tetragonally distorted octahedral sites.

The morphologies of ZGC and ZGO were characterized by TEM (Fig. 1a and i). The ZGC and ZGO samples had similar morphology and size. The ZGC showed an average size of 7.7 ± 1.5 nm (N = 100, Fig. S5). The microstructures consisted of numerous hexagonal shapes, implying that they had exposed crystal facets of the (1 1 1) plane. To investigate the structural details of the as-prepared ZGC and ZGO, HRTEM, the corresponding FFT, IFFT images, and line-scan height profiles were analysed (Fig. 1a–e and Fig. 1i–m). The results show that ZGC and ZGO had similar lattice fringes, corresponding to (1 1 1) and (3 1 1) lattice planes on ZGO nanoparticle, respectively. However, ZGC exhibited smaller d-spacing of the (1 1 1) and (3 1 1) planes than ZGO (Fig. 1c–e and 1 k-m), revealing the lattice shrinkage in ZGC, which was consistent with the peak shift to higher angles in the XRD patterns (Fig. 1f and g). These results suggest that the Cu doping decreased the interatomic spacing.

N_2 adsorption/desorption isotherms of ZGO and ZGC were obtained to measure the specific surface area (Fig. S6). Typical type-IV curves were observed both in N_2 adsorption/desorption isotherms of ZGO and ZGC, indicating the presence of mesopores in the dendrites. The Brunauer-Emmett-Teller (BET) surface area of ZGC (100.5 m^2/g) was nearly equal to that of ZGO (99.9 m^2/g). The results show that Cu(II) doping did not lead to significant difference in specific surface area.

Oxygen vacancies (Ov) with defect states can trap e^- or h^+, which is conducive to photocatalytic efficiency and change the binding energies [31]. Therefore, XPS analysis was performed to reveal the chemical states of the oxygen elements in the prepared ZGO and ZGC. The O 1 s spectra of both ZGO and ZGC could be deconvoluted into three sub-peaks at 530.3 ± 0.1, 531.6 ± 0.1, and 533.0 ± 0.1 eV (Fig. S7), corresponding to lattice oxygen atoms in a fully-coordinated environment (O_I), lattice oxygen atoms in the vicinity of Vo (O_{II}), and surface-adsorbed species (O_{III}), respectively [32,33]. Cu(II) doping made the relative intensity of O_{II} increase, but reduced that of O_{III} (Fig. S8). This phenomenon can be ascribed to the generation of more Vos in ZGC than ZGO [34–36].

3.2. Optical properties of ZGC nanoparticles

PL spectra were acquired to study whether the separation of photo-generated charge carriers was facilitated by Cu(II) doping. The excitation (Ex) and emission spectra (Em) of ZGO and ZGC are shown in Fig. 2a. The maximum emission peak located around 700 nm originating from the Vo, and a weak emission peak appeared around 510 nm belonging to the ^2E_A- $^4A_2$ transition of Ga^{3+} in the distorted octahedral (inset of Fig. 2a) [32,37]. Both ZGO and ZGC gave similar PL bands, but ZGC showed much weaker PL signal due to the effective inhibition of the recombination of the photo-generated e^--h^+ pairs. The above results suggest that Cu(II) doping greatly assisted the separation of photo-generated charge carriers in favor of the next photocatalytic degradation.

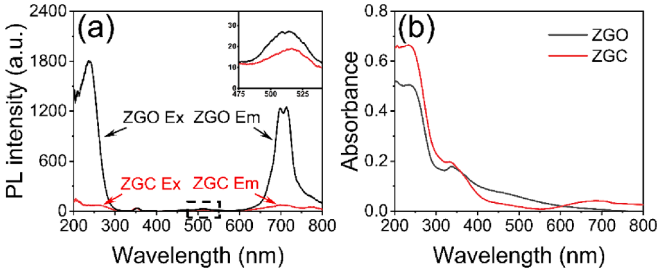

Fig. 2. Optical properties of ZGO and ZGC nanoparticles. (a) PL spectra, inset: amplified PL spectra in the range marked in black dotted box. (b) UV–vis diffuse reflectance spectra.

UV–vis diffuse reflectance spectra were measured to study the effect of Cu(II) doping on the optical absorption properties of ZGO due to the change of the electronic structure. As is shown in Fig. 2b, both ZGO and ZGC exhibited similar absorption edges around the ultraviolet region with strong absorption below 500 nm. ZGC gave an additional trailing absorption over 500 nm resulting from a typical light absorption process of defect states. In particular, a red shift of the absorption band edge in conjunction with a significant absorption enhancement was distinctly observed for ZGC. The result indicates the preferable adsorption of the UV and NIR lights by ZGC.

To explore the behaviour of photogenerated charge carriers, the time-resolved photoluminescence spectra were collected to analyse the lifetime of photogenerated carriers (Fig. S9 and Table S1). ZGO and ZGC gave the average lifetime of 1.5 and 8.7 ms for photogenerated carriers, respectively, suggesting ZGC enabled more effective migration and separation of interfacial charges [38]. As a result, Cu(II) doping significantly prolonged the lifetime of photogenerated carriers.

Raman spectra were collected to further reveal the doping situation of Cu(II) ions. ZGO and ZGC gave similar Raman profiles (Fig. S10). The peaks at 610 cm^{-1} (T_{2g}) and 716 cm^{-1} (A_{1g}) were related to the asymmetric stretching vibration and the symmetric ZnO_4 tetrahedron [39]. Compared with ZGO, ZGC gave weaker intensity of T_{2g} and showed a slight left-shift of the A_{1g} peak, indicating Cu(II) doping resulted in octahedral distortion and asymmetrical ZnO_4 tetrahedron [40].

3.3. ROS generation analysis

To detect the ROS production by the pre-illuminated ZGO and ZGC in the dark, DCFH, which can be oxidized to DCF by ROS to give strong fluorescence at 525 nm, was chosen as the fluorescence probe [23]. As shown in Fig. 3a, in the presence of DCFH, pre-illuminated ZGC gave much stronger fluorescence than pre-illuminated ZGO because Cu(II) doping made ZGC have excellent photo-energy trapping capacity and efficient releasing of photo-generated e^- and h^+ pairs to the surface for ROS generation. Moreover, the fluorescence intensity of DCF increased with pre-illuminated ZGC concentration (Fig. 3b) and pre-illumination time (Fig. 3c). The results indicate the ROS production of pre-illuminated ZGC was dependent of ZGC concentration and pre-illumination time.

The persistent ROS production capacity of pre-illuminated ZGC was also explored. As shown in Fig. 3d, the fluorescence of ZGC dispersion with DCFH indicator was continuously detected for 96 h, suggesting the remarkable persistent photocatalytic activity of pre-illuminated ZGC. The above results demonstrate the great significance of Cu(II) doping into ZGO in improving ROS production for persistent photodegradation.

3.4. Detection of specific reactive species

Previous studies have proven that e^-, h^+ and various reactive radical intermediate species are generated during the photocatalytic process, such as hydroxyl radicals (•OH), $•O_2^-$, and $^1O_2$ [5]. To further verify the formation of active species generated by the as-prepared ZGO and ZGC after pre-illumination, EPR spectroscopy was used to record the free radicals with or without pre-illumination by 254 nm UV light. Firstly, DMPO was chosen to verify the generation of •OH/•H and $•O_2^-$. Fig. S11a shows a characteristic 9-fold signal of DMPO-•H adduct, and the 6-fold signal of the carbon-centered radical, but no typical 1:2:2:1 quartet characteristic signal of DMPO-•OH adduct. This situation could

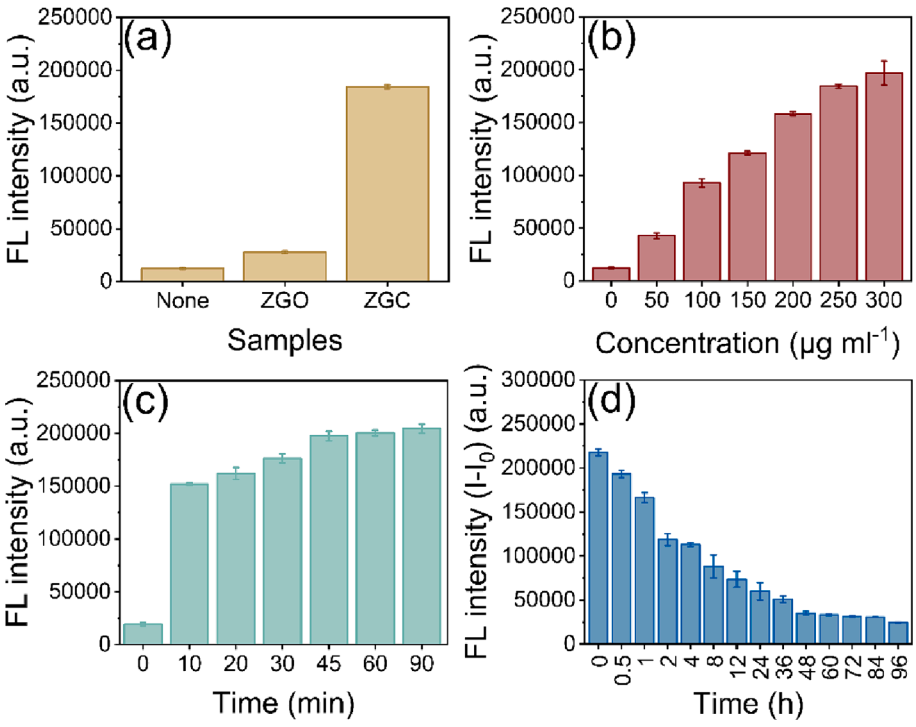

Fig. 3. Fluorescence intensities of DCFH exposed to (a) 250 μg mL^{-1} of ZGO and ZGC dispersion after pre-illumination by a 254 nm UV lamp for 60 min, (b) various concentrations of ZGC dispersions with pre-illumination by a 254 nm UV lamp for 60 min, (c) 250 μg mL^{-1} ZGC dispersion with pre-illumination by a 254 nm UV lamp for different periods, and (d) 250 μg mL^{-1} ZGC dispersion at various time points after pre-illumination by a 254 nm UV lamp for 60 min. Error bars, ± one standard deviation, n = 3.

be attributed to a relatively high reaction rate to efficiently consume •OH including the partial transformation of •OH to •H [41,42]. The un-illuminated ZGC also generated •H but with a small amount. Fig. S11b showed a weak DMPO-$•O_2^-$ signal in the pre-illuminated ZGC, confirming the generation of $•O_2^-$.

TEMP was further used to trap $^1O_2$. As presented in Fig. S11c, no signal was detected in un-illuminated ZGC. However, pre-illuminated ZGC showed three peaks with stronger intensity in a 1:1:1 ratio than pre-illuminated ZGO, suggesting that Cu(II) doping enhanced the generation of $^1O_2$ after pre-illumination.

TEMPO was used as a spin label to detect the generated h^+. As TEMPO itself has EPR signal, so the blank group with TEMPO showed obvious signal. The obvious decrease in the signal intensity of TEMPO in pre-illuminated ZGC indicates the formation of h^+. As shown in Fig. S11d, pre-illuminated ZGC gave a more significant decrease in the signal intensity than pre-illuminated ZGO, revealing the generation of more h^+ from pre-illuminated ZGC.

3.5. Persistent photocatalytic degradation of dyes

To evaluate the persistent photocatalytic ability of the as-prepared nanoparticles, the persistent decomposition curves of RhB were measured in an aqueous solution in the dark. The as-prepared photocatalyst powders were first irradiated with a UV lamp for 60 min and then placed into the RhB solution for degradation application in the dark. For comparison, degradation experiments for the as-prepared photocatalyst powders without any pre-illumination were also carried out under the same conditions. As shown in Fig. 4a, un-illuminated ZGO and ZGC gave similar degradation results, indicating the insignificant impact of the doped Cu(II) on the degradation of RhB under dark conditions without pre-illumination. About 35.3 % and 32.2 % of RhB degraded by un-illuminated ZGO and ZGC in 60 min, respectively, mainly because they can generate •H even under dark conditions from the EPR data (Fig. S11a). In contrast, pre-illuminated ZGC made RhB degrade immediately, whereas pre-illuminated ZGO had RhB degrade after 20 min, indicating Cu doping accelerated the persistent degradation. Moreover, pre-illuminated ZGC exhibited a significantly higher degradation efficiency (82.2 % of RhB degraded in 60 min) in the dark than pre-illuminated ZGO (49.6 % of RhB degraded in 60 min). The results show that Cu(II) doping greatly enhanced the overall catalytic performance in the dark after pre-illumination due to the introduction of more photogenerated carriers.

Compared to other persistent photocatalytic materials [9,18,21,43], ZGC gave much faster and efficient persistent degradation of organic dyes (82.2 % of RhB degraded in 60 min) with a small size of 7.5 ± 1.5 nm and lower irradiation power intensity (Table 1).

To understand the contribution of the generated active species (•OH, $•O_2^-$, $^1O_2$ and h^+) to persistent photocatalytic degradation, capture experiments for various active species were carried out. IPA, BQ, AO and L-His were used to trap •OH, $•O_2^-$, h^+ and $^1O_2$, respectively. The persistent photodegradation of RhB in the presence of un-illuminated ZGO and ZGC were inhibited by IPA (Fig. 4b), while pre-illuminated ZGC was significantly inhibited by IPA, AO, and L-His followed the order of IPA > AO ~ L-His (Fig. 4c), indicated the significance of •OH. The EPR data showed the active species was •H, which was linked to the transformation of •OH to •H. Therefore, •H played a vital role while h^+ and $^1O_2$ a secondary role in the persistent photocatalysis. The same is also true for the dominant ROS in the persistent photodegradation process of ZGO (Fig. 4d), but h^+ and $^1O_2$ showed more significant effects in ZGC (Fig. 4c). In general, BQ gave no obvious inhibition, indicating the insignificant contribution of $•O_2^-$ to the degradation of RhB.

To show the persistent catalytic behaviour of ZGC for organic pollutants, other three dyes were chosen as target pollutants. It is well known that RhB, CV, and MB are cationic dyes and MO is an anionic dye [44,45]. Although the surface of ZGC is negatively charged (Fig. S12), ZGC showed no interaction with cationic MB dye, but acted as photocatalyst for degrading anionic MO dye as well as RhB and CV dyes (Fig. S13-S16). Thus, the main driving force for the decrease of the

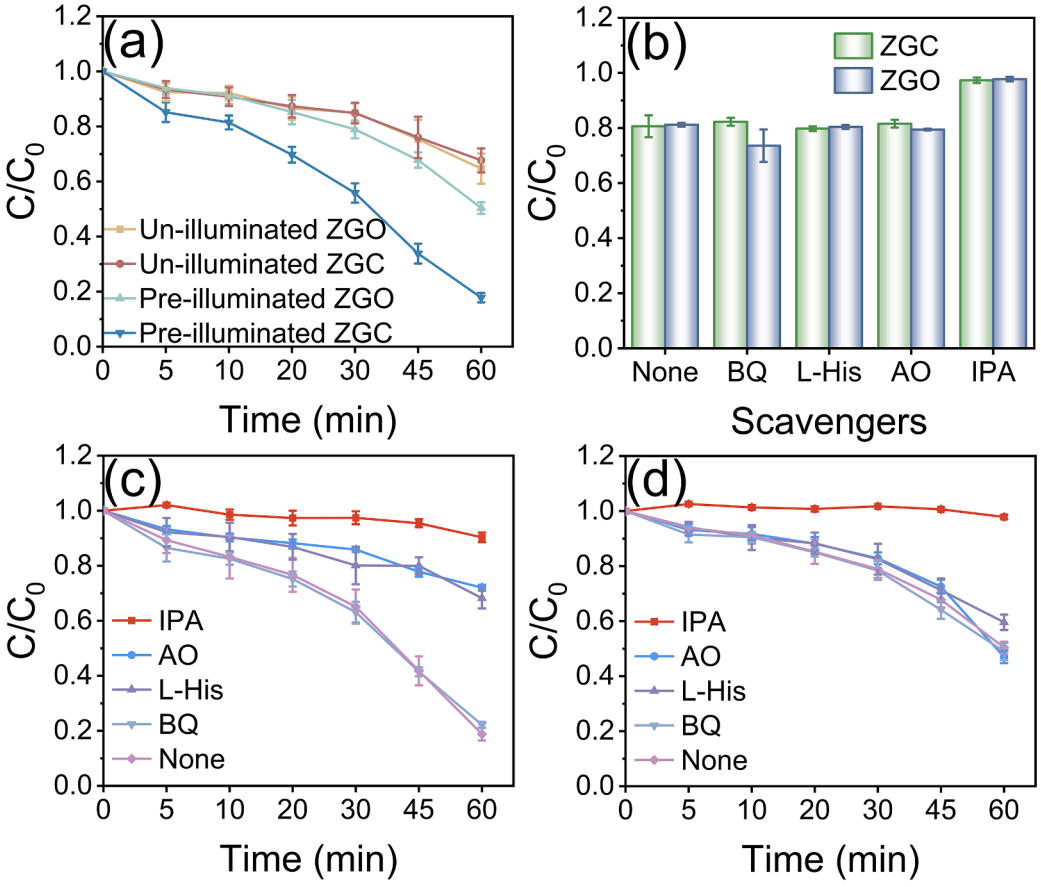

Fig. 4. Persistent photocatalytic activity for RhB degradation: (a) ZGO and ZGC with or without 254 nm UV light pre-illumination for 60 min; (b) trapping experiments of active species by un-illuminated ZGO and ZGC after reaction in the dark for 30 min; (c) trapping experiments of active species from pre-illuminated ZGC; (d) trapping experiments of active species from pre-illuminated ZGO. Error bars, ± one standard deviation, n = 3. BQ, L-His, AO and IPA were used to trap $\bullet O_2^-$, $^1O_2$, h^+ and •OH, respectively.

Table 1
Comparison of over reported persistent photocatalytic materials for degradation of organic pollutants in the dark environment.

Catalysts	Pollutants	Pollutant concentration (mg/L)	Particle size	Light source	Active species	Degradation efficiency	Ref.
$MgGa_2O_4$	RhB	20	400 nm long × 100 nm wide	500 W UV lamp	•OH	31 % in 1 h	[9]
$ZnGa_2O_4:Cr^{3+}$-750- EDTA	MB MG CV	50 30 5	20 nm	30 W LED	•OH, $\bullet O_2^-$, h^+	59.9 % in 10 h 95 % in 10 h 95 % in 10 h	[18]
$Sr_2MgSi_2O_7:Eu^{2+},Dy^{3+}$	MO RhB MB	20	micron-sized	250 W mercury lamp	•OH,$\bullet O_2^-$	39.5 % in 24 h 76.5 % in 24 h 20.4 % in 24 h	[21]
MI-$ZnGa_2O_4:Cr^{3+}$-750-EDTA	TC OTC MG	25 25 50	20 nm	500 W Xe lamp, λ ≥ 420	•OH, $\bullet O_2^-$, h^+	11.6 % in 4 h 10.5 % in 4 h 18.5 % in 4 h	[43]
$ZnGa_2O_4:Cu^{2+}$	RhB	10	7.7 nm	6 W UV lamp	•H, $^1O_2$, h^+	82.2 % in 1 h	This work

Notes: EDTA, MG, TC, OTC and MI are the abbreviations of ethylenediaminetetraacetic acid disodium, malachite green, tetracycline, oxytetracycline and molecular-imprinting, respectively.

solution concentration of dyes was photocatalytic degradation rather than electrostatic attraction. Fig. S17 shows the structures of the four dyes. MO has a visible part of the spectra with a maximum of 465 nm originating from a conjugated structure formed by the N═N azo bond (chromophore) [46]. The azo bond is a potential reaction site for •H and cationic dyes are reduced by •H preferentially at the $C{=}N^+$ bond [41], so the anionic MO dye with N═N azo bond, RhB, and CV with the $C{=}N^+$ bond degraded in the presence of ZGC. However, ZGC showed no photocatalytic effect on MB due to the lack of the $C{=}N^+$ bond.

Wastewater often contains more than one dye. The persistent decomposition of the RhB-MB-MO-CV mixture solution was examined in the presence of pre-illuminated ZGC in the dark. For this purpose, the UV–vis absorption spectra of the mixture solution in the dark were measured at 30 min after pre-illuminated or unilluminated ZGC was added. The absorption peaks of the RhB-MB-MO-CV mixture solution were the superposition of those of RhB, MB, MO and CV (Fig. S18). All

the dyes in the mixture underwent photodegradation with the pre-illuminated ZGC, but the degradation of dye mixture was less significant than single dyes due to the competitive photodegradation between the dyes. The degradation efficiency followed an decreasing order of MO > RhB > CV > MB. These results further confirm the efficient persistent photocatalytic activity of ZGC towards organic pollutants in the case of dark or slight light conditions.

3.6. Reusability of ZGC

The long-term stability of photocatalysts is a crucial consideration for their practical applications. To assess its stability for practical use, ZGC was washed and collected, and four recycled experiments were conducted to evaluate its persistent photocatalytic degradation for RhB under identical conditions. As shown in Fig. S19, the persistent photocatalytic performance of ZGC did not decrease after four recycles of degradation experiments. Additionally, the XRD pattern revealed that the crystal phase of the fourth recycled ZGC remained unchanged (Fig. S20). These results indicate that ZGC had excellent persistent photocatalytic stability for the degradation of organic dyes.

3.7. Persistent photocatalytic mechanism of ZGC

Density functional theory calculation was conducted to investigate the band structure and state density of ZGO and ZGC. As shown in Fig. 5a, the valence band of ZGO was predominantly composed of O 2p orbitals and hybridized with a minor contribution from Zn 3d and Ga 3d orbitals, while the conduction band mainly constituted O 2p orbitals. Once the lattice Ga(III) ions in ZGO were substituted by doped Cu(II) ions, the electronic orbitals of the doped Cu(II) ions engaged in hybridization with the GaO_6 octahedron [17], so the Cu 3d states also played a role in the formation of the valence band in ZGC. A new energy level stemming from Cu 3d and O 2p states was found (Fig. 5b), indicating that Cu(II) could serve as an efficient trap center with suitable depth. Consequently, in addition to electron transition from the valence band to the conduction band, there is also a transition of e^- from the valence band to the energy level of the doped Cu(II) ions [47].

Fig. 6 illustrates the mechanism for the persistent photocatalysis of ZGC after stopping excitation. ZGO is a type of long afterglow matrix material, possess two active centers, luminescent center and trap center. The luminescent center can facilitate the recombination of e^- and h^+, which is conducive to afterglow luminescence. The trap center can store and release photo-generated charge carriers. The doped Cu(II) ions serve as the trap center rather than luminescent center inhibit the recombination of e^- and h^+ to promote the production of active species. The potential persistent catalytic mechanisms of ZGC are associated with the involved active species (•OH, •H, $•O_2^-$, $^1O_2$ and h^+). When ZGC is irradiated by UV light with an energy greater than or equal to the band gap energy, e^- and h^+ are generated (eq 1), and stored in traps [10,48]. These stored e^- and h^+ can be continuously released from the traps for a period in the dark, subsequently transferred to the surface of ZGC, where they respectively oxidize H_2O molecules into H^+ and •OH (eq 4), and reduced oxygen into $•O_2^-$ (eq 2) [49]. Moreover, $•O_2^-$ is oxidized by h^+ to generate $^1O_2$ (eq 3) and the •OH transformed to •H (eq 5) [41,50]. The obtained •H, $•O_2^-$, $^1O_2$ and h^+ act as strong oxidizing agents to effectively degrade the organic dyes (eq 6). The stoichiometry dominating degradation reaction for ZGC is as follows:

$$ZGC + hv \rightarrow h^+_{VB} + e^-_{CB} \quad (1)$$

$$O_2 + e^-_{CB} \rightarrow •O_2^- \quad (2)$$

$$•O_2^- + h^+_{VB} \rightarrow {}^1O_2 \quad (3)$$

$$H_2O + h^+_{VB} \rightarrow • OH + H^+ \quad (4)$$

$$•OH \rightarrow •H \quad (5)$$

$$\text{Organic dye} + (•H, {}^1O_2, h^+) \rightarrow CO_2 + H_2O \quad (6)$$

4. Conclusions

In summary, we have reported the excellent ability of ZGC nanoparticles for persistent photocatalytic degradation of organic dyes with good recycling capability. The replacement of Ga(III) sites by Cu(II) doping did not change the crystal structure, but significantly improved the production and availability of active species. The doped Cu(II) ions acted as trapping sites to greatly increase the charge transfer rate, and promote the long lifetime release and separation of e^- and h^+ pairs. •H played a vital role while h^+ and $^1O_2$ played secondary roles in the persistent degradation of organic dyes in the dark. ZGC nanoparticles

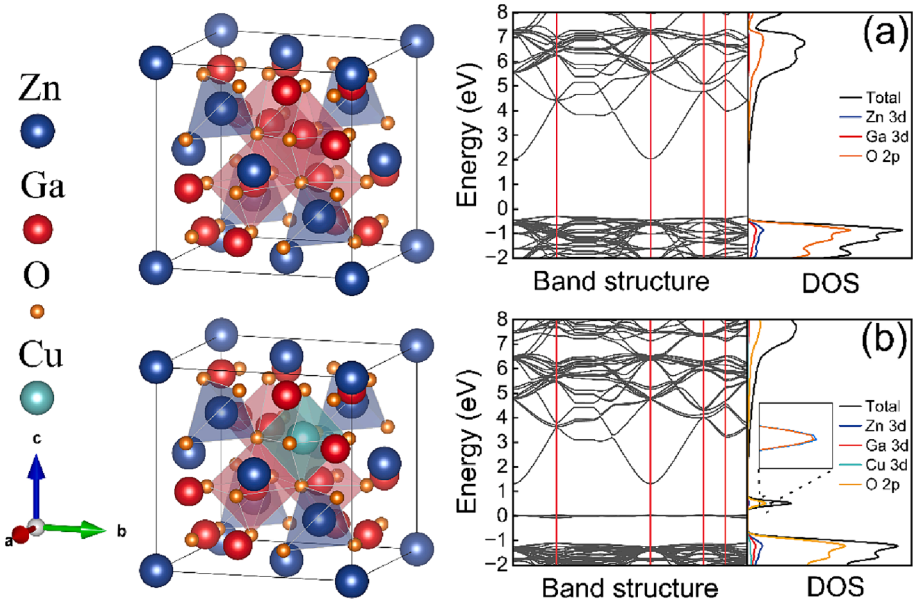

Fig. 5. Model, band structure, and density of states (DOS) of the as-prepared nanoparticles ZGO (a) and ZGC (b).

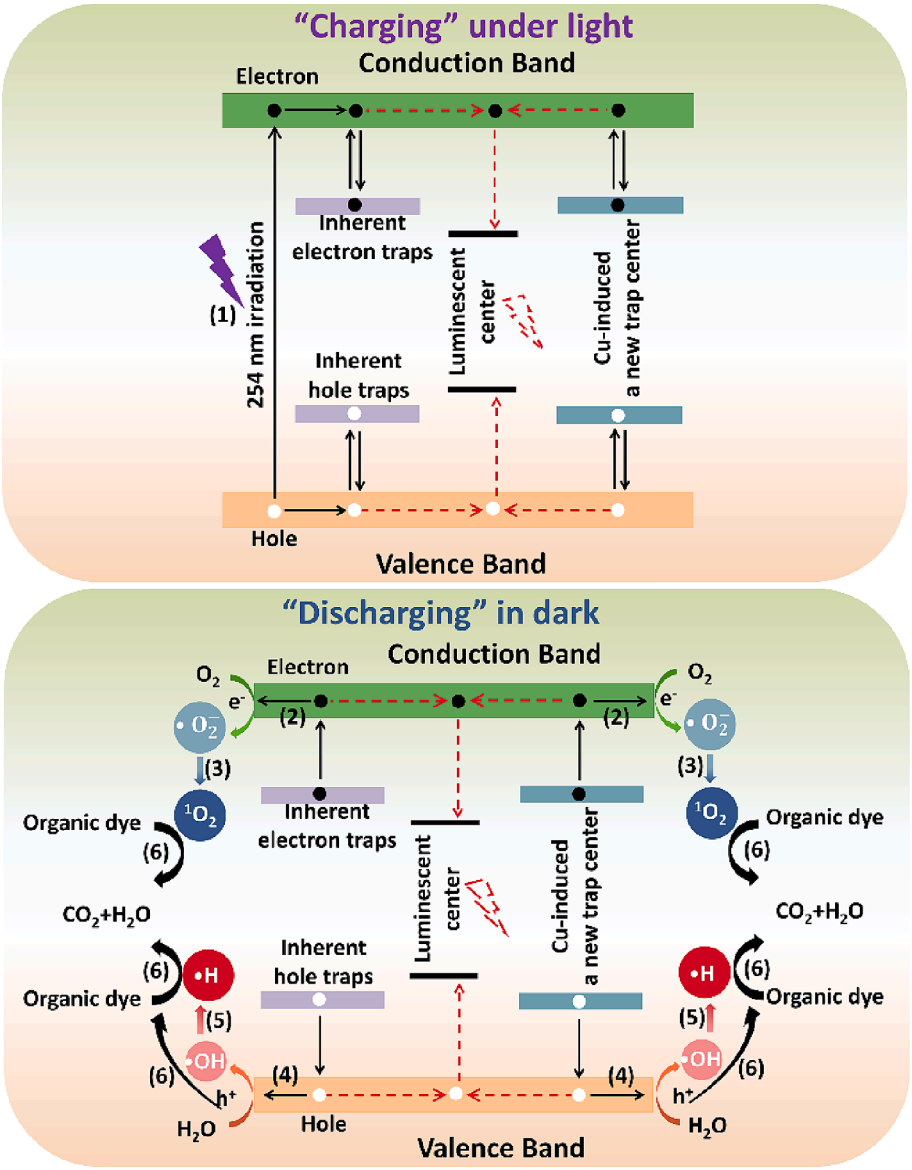

Fig. 6. Mechanism illustration for the persistent photocatalysis of ZGC after stopping excitation.

exhibited much higher efficiency and more rapid degradation of organic dyes than other persistent photocatalytic materials [9,18,21,43]. This investigation highlights the potential of ZGC as a persistent photocatalyst for the degradation of organic pollutants in the case of dark or slight light conditions.

Author contribution

Dong-Mei Zhou: Investigation, methodology, data curation, formal analysis, writing- original draft. **Li-Jian Chen:** Conceptualization, validation, supervision, writing-review and editing. **Xu Zhao:** Methodology, formal analysis, funding acquisition. **Li-Xia Yan:** Methodology, formal analysis, funding acquisition. **Xiu-Ping Yan:** Project administration, conceptualization, supervision, writing – review and editing, funding acquisition.

CRediT authorship contribution statement

Dong-Mei Zhou: Writing – original draft, Methodology, Investigation, Formal analysis, Data curation. **Li-Jian Chen:** Writing – review & editing, Validation, Supervision, Conceptualization. **Xu Zhao:** Methodology, Funding acquisition, Formal analysis. **Li-Xia Yan:** Methodology, Funding acquisition, Formal analysis. **Xiu-Ping Yan:** Writing – review & editing, Supervision, Project administration, Conceptualization.

Declaration of competing interest

The authors declare that they have no known competing financial interests or personal relationships that could have appeared to influence the work reported in this paper.

Data availability

Data will be made available on request.

Acknowledgements

This work was supported by the National Natural Science Foundation of China (No. 21934002, 22304063), Natural Science Foundation of Jiangsu Province, China (No. BK20231491) and the Collaborative Innovation Center of Food Safety and Quality Control in Jiangsu

Province.

Appendix A. Supplementary material

Supplementary material to this article can be found online at https://doi.org/10.1016/j.jcis.2024.04.135.

References

[1] X. Hou, L. Mu, F. Chen, X.G. Hu, Emerging investigator series: design of hydrogel nanocomposites for the detection and removal of pollutants: from nanosheets, network structures, and biocompatibility to machine-learning-assisted design, Environ Sci.-Nano 5 (2018) 2216–2240.

[2] Y.P. Zhou, F.S. Zeng, C.Y. Sun, J. Wu, Y. Xie, F.Y. Zhang, S.L. Rao, F.H. Wang, J. B. Zhang, J.S. Zhao, S.Q. Li, Gd_2O_3 nanoparticles modified g-C_3N_4 with enhanced photocatalysis activity for degradation of organic pollutants, J. Rare Earths 39 (2021) 1353–1361.

[3] Q.D. Liu, J. Hou, J. Wu, L.Z. Miao, G.X. You, Y.H. Ao, Intimately coupled photocatalysis and biodegradation for effective simultaneous removal of sulfamethoxazole and COD from synthetic domestic wastewater, J. Hazard. Mater. 423 (2022) 11.

[4] C.C. Dong, W.Z. Fang, Q.Y. Yi, J.L. Zhang, A comprehensive review on reactive oxygen species (ROS) in advanced oxidation processes (AOPs), Chemosphere 308 (2022) 18.

[5] J.L. Liu, G.H. Dong, J. Jing, S.Y. Zhang, Y. Huang, K. Ho, Photocatalytic reactive oxygen species generation activity of TiO_2 improved by the modification of persistent free radicals, Environ Sci.-Nano 8 (2021) 3846–3854.

[6] P.P. Gai, W. Yu, H. Zhao, R.L. Qi, F. Li, L.B. Liu, F.T. Lv, S. Wang, Solar-powered organic semiconductor-bacteria biohybrids for CO_2 reduction into acetic acid, Angew. Chem.-Int. Edit. 59 (2020) 7224–7229.

[7] G.M. Su, R.C. Shen, J. Tan, Q. Yuan, Progress on the application of long persistent phosphors in photocatalytic system, Chem. J. Chin. Univ.-Chin. 41 (2020) 2404–2414.

[8] P.F. Feng, Y.D. Wei, Y.N. Wang, J.C. Zhang, H.H. Li, Z.P. Ci, Long persistent phosphor $CdSiO_3$:Gd^{3+}, Bi^{3+} and potential photocatalytic application of $CdSiO_3$:Gd^{3+}, Bi^{3+}@TiO_2 in dark, J. Am. Ceram. Soc. 99 (2016) 2368–2375.

[9] P.F. Feng, J.P. Zhao, J.C. Zhang, Y.D. Wei, Y.N. Wang, H.H. Li, Y.H. Wang, Long persistent photocatalysis of magnesium gallate nanorodes, J. Alloy. Compd. 695 (2017) 1884–1890.

[10] M. Sakar, C.C. Nguyen, M.H. Vu, T.O. Do, Materials and mechanisms of photo-assisted chemical reactions under light and dark conditions: can day-night photocatalysis be achieved? ChemSusChem 11 (2018) 809–820.

[11] X.M. Yang, J.M. Ma, R. Guo, X.C. Fan, P. Xue, X.Z. Wang, H. Sun, Q.F. Yang, X. Y. Lai, Ordered mesoporous $ZnGa_2O_4$ for photocatalytic hydrogen evolution, Mat. Chem. Front. 5 (2021) 5790–5797.

[12] H.L. Shen, J. He, X.Q. Shao, Q. Su, D.L. Zhao, S.J. Feng, Effect of partial substitution of Zn^{2+} with Co^{2+} on catalytic methane combustion performance of $Zn_{1-x}Co_xGa_2O_4$ (x=0, 0.1, 0.3) microspheres, Solid State Sci. 118 (2021) 6.

[13] W.W. Zhang, J.Y. Zhang, X.A. Lan, Z.Y. Chen, T.M. Wang, Photocatalytic performance of $ZnGa_2O_4$ for degradation of methylene blue and its improvement by doping with Cd, Catal. Commun. 11 (2010) 1104–1108.

[14] X.P. Bai, X. Zhao, W.L. Fan, Preparation and enhanced photocatalytic hydrogen-evolution activity of $ZnGa_2O_4$/N-rGO heterostructures, RSC Adv. 7 (2017) 53145–53156.

[15] J. Liang, Y. Chai, L. Li, D.L. Li, J.N. Shen, Y.F. Zhang, X.X. Wang, Germanium and iron double-substituted $ZnGa_2O_4$ solid-solution photocatalysts with modulated band structure for boosting photocatalytic CO_2 reduction with H_2O, Appl. Catal. B-Environ. 265 (2020) 118551.

[16] J. Liu, W. Lu, H.Z. Wu, L. Jin, B. Hu, L.L. Li, Z.L. Wang, In situ synthesis of rice-like $ZnGa_2O_4$ for the photocatalytic removal of organic and inorganic pollutants, Mater. Sci. Semicond. Process 56 (2016) 251–259.

[17] Z.J. Shi, D.K. Shi, L.X. Zhang, Y. Cao, Regulating the band structure by modifying Ti_3C_2 and doping Fe ions improved photocatalytic activity and selectivity of $ZnGa_2O_4$-Ti_3C_2-Fe for photoreducted CO_2 into CH_4, J. Power Sources 535 (2022) 11.

[18] Y. Zhang, Z.W. Wang, X. Ji, T. Wang, X.T. Yang, H.F. Wang, Afterglow-catalysis and self-reporting of pollutant degradation by ethylenediaminetetraacetic acid disodium-etched Cr:$ZnGa_2O_4$, J. Phys. Chem. C 125 (2021) 9096–9106.

[19] D.L. Han, Y.J. Han, J. Li, X.M. Liu, K.W.K. Yeung, Y.F. Zheng, Z.D. Cui, X.J. Yang, Y.Q. Liang, Z.Y. Li, S.L. Zhu, X.B. Yuan, X.B. Feng, C. Yang, S.L. Wu, Enhanced photocatalytic activity and photothermal effects of cu-doped metal-organic frameworks for rapid treatment of bacteria-infected wounds, Appl. Catal. B-Environ. 261 (2020) 118248.

[20] J.H. Gong, L.J. Chen, X. Zhao, X.P. Yan, Persistent production of reactive oxygen species with Zn_2GeO_4: Cu nanorod-loaded microneedles for methicillin-resistant staphylococcus aureus infectious wound healing, ACS Appl. Mater. Interfaces 14 (2022) 17142–17152.

[21] O. Hai, M.K. Pei, E.L. Yang, Q. Ren, X.L. Wu, J.F. Zhu, Y.J. Zhao, L. Du, Exploration of long afterglow luminescence materials work as round-the-clock photocatalysts, J. Alloy. Compd. 866 (2021) 158752.

[22] C.F. Chen, C.C. Zhang, Y.N. Zhang, H.J. Shang, Y.H. Shao, H.Y. Liu, C.S. Pan, Boosting H_2O_2 generation by shortening the charge migration distance in $BiPO_4$ nanocrystals, J. Colloid Interface Sci. 662 (2024) 1–10.

[23] L.L. Liu, J.F. Huang, L.Y. Cao, J.P. Wu, J. Fei, H.B. Ouyang, F.L. Ma, C.J. Zhou, Synthesis of $ZnGa_2O_4$ octahedral crystallite by hydrothermal method with the aid of CTAB and its photocatalytic activity, Mater. Lett. 95 (2013) 160–163.

[24] Z.H. Li, J. Wang, R.C. Shen, N. Chen, X.Y. Qin, W.J. Wang, Q. Yuan, Topological radiated dendrites featuring persistent bactericidal activity for daily personal protection, Small 17 (2021) 9.

[25] D. Bidwai, N.K. Sahu, S.J. Dhoble, A. Mahajan, D. Haranath, G. Swati, Review on long afterglow nanophosphors, their mechanism and its application in round-the-clock working photocatalysis, Methods Appl. Fluoresc. 10 (2022) 30.

[26] Z.J. Li, Y.W. Zhang, X. Wu, L. Huang, D.S. Li, W. Fan, G. Han, Direct aqueous-phase synthesis of sub-10 nm "luminous pearls" with enhanced in vivo renewable near-infrared persistent luminescence, J. Am. Chem. Soc. 137 (2015) 5304–5307.

[27] X.Y. Guo, S. Liu, W.J. Wang, C.T. Zhu, C.Y. Li, Y. Yang, Q.H. Tian, Y. Liu, Enhanced photocatalytic hydrogen production activity of Janus $Cu_{1.94}S$-ZnS spherical nanoheterostructures, J. Colloid Interface Sci. 600 (2021) 838–846.

[28] A. Meyer, G. Schnakenburg, R. Glaum, O. Schiemann, (Bis(terpyridine))copper(II) Tetraphenylborate: a complex example for the Jahn-Teller Effect, Inorg. Chem. 54 (2015) 8456–8464.

[29] V.L. Matukhin, V.A. Ulanov, A.A. Sukhanov, A.N. Safonov, S.V. Shmidt, T. G. Aminov, G.G. Shabunina, Investigation of $CuGaTe_2$ semiconductor compounds doped with Mn by the EPR method, Russ. Phys. J. 54 (2011) 283–287.

[30] I.T. Papadas, C. Kosma, Y. Deligiannakis, Ternary Al_2O_3-electrolyte-Cu^{2+} species: EPR spectroscopy and surface complexation modeling, J. Colloid Interface Sci. 339 (2009) 19–30.

[31] Y.M. Huang, Y. Yu, Y.F. Yu, B. Zhang, Oxygen vacancy engineering in photocatalysis, Sol. RRL 4 (2020) 14.

[32] W.J. Yang, J. Li, B.D. Liu, X.L. Zhang, C. Zhang, P.J. Niu, X. Jiang, Multi-wavelength tailoring of a $ZnGa_2O_4$ nanosheet phosphor via defect engineering, Nanoscale 10 (2018) 19039–19045.

[33] M.A. Mahadik, H.H. Lee, W.S. Chae, M. Cho, J.S. Jang, Energy-efficient photoelectrochemical water splitting and degradation of organic dyes over microwave-assisted WO_3 nanosheets/W foil with rapid charge transport, Sol. Energy Mater. Sol. Cells 246 (2022) 13.

[34] G.W. An, L.K. Dhandole, H. Park, H.S. Bae, M.A. Mahadik, J.S. Jang, Enhanced charge transfer process in morphology restructured TiO_2 nanotubes via hydrochloric acid assisted one step-in-situ hydrothermal approach, ChemCatChem 11 (2019) 5606–5614.

[35] H.S. Bae, R.P. Patil, J. Ha Hwang, M.A. Mahadik, M.S. Song, W.S. Chae, V. Manikandan, J.S. Jang, Visible-light-responsive hydrogen-reduced CoOx loaded Rh/Sb:$SrTiO_3$ nanocubic photocatalyst for degradation of organic pollutants and inactivation of bacteria, J. Environ Chem. Eng. 11 (2023) 12.

[36] I.S. Hwang, M.A. Mahadik, H.H. Lee, S.H. Choi, J.S. Jang, Synchronized surface oxygen states and electron-hole passage in microwave-assisted tungsten oxide for photocatalytic organic decomposition and antibacterial activity, J. Environ. Chem. Eng. 10 (2022) 13.

[37] D.R. Li, Y.H. Wang, K. Xu, H. Zhao, Z.F. Hu, Persistent luminescent and photocatalytic properties of $ZnxGa_2O_{3+x}$ ($0.8 \leq x \leq 1$) phosphors, RSC Adv. 5 (2015) 20972–20975.

[38] W. Zhao, S.Y. Liu, Y. Liu, S. Yang, B.Z. Liu, X.K. Hong, J.Y. Shen, C. Sun, Integration of ohmic junction and step-scheme heterojunction for enhanced photocatalysis, J. Colloid Interface Sci. 654 (2024) 134–149.

[39] Y. Xiong, H.Y. Xie, Z.G. Rao, L.J. Liu, Z.F. Wang, C.C. Li, Compositional modulation in $ZnGa_2O_4$ via Zn^{2+}/Ge^{4+} co-doping to simultaneously lower sintering temperature and improve microwave dielectric properties, J. Adv. Ceram. 10 (2021) 1360–1370.

[40] E. Chikoidze, C. Sartel, I. Madaci, H. Mohamed, C. Vilar, B. Ballesteros, F. Belarre, E. del Corro, P. Vales-Castro, G. Sauthier, L.J. Li, M. Jennings, V. Sallet, Y. Dumont, A. Pérez-Tomás, P-type ultrawide-band-gap spinel $ZnGa_2O_4$: new perspectives for energy electronics, Cryst. Growth Des. 20 (2020) 2535–2546.

[41] J.L. Peng, K. Du, J. Sun, X.L. Yang, X. Wang, X.R. Zhang, G. Song, F.D. Feng, Photocatalytic generation of hydrogen radical (H) with GSH for photodynamic therapy, Angew. Chem.-Int. Edit. 9 (2023) 62.

[42] Q.J. Wang, J.Y. Wang, W.J. Rui, D. Yang, X.Y. Wan, C.M. Zhou, R.H. Li, W. Liu, Y. H. Dai, Y.H. Yang, Metal-carbonate interface promoted activity of Ag/$MgCO_3$ catalyst for aqueous-phase formaldehyde reforming into hydrogen, Fuel 337 (2023) 8.

[43] Y. Zhang, Z.W. Wang, X.T. Yang, Y.Z. Zhu, H.F. Wang, Afterglow-catalysis and molecular imprinting: a promising union for elevating selectivity in degradation of antibiotics, Appl. Catal. B-Environ. 305 (2022) 121025.

[44] X. Ji, Y. Guo, S.G. Hua, H.Y. Li, S.C. Zhang, Interaction-determined sensitization photodegradation of dye complexes by boron nitride under visible light irradiation: experimental and theoretical studies, New J. Chem. 44 (2020) 9238–9247.

[45] Y.X. Xue, Q.Q. Chang, X.Y. Hu, J. Cai, H. Yang, A simple strategy for selective photocatalysis degradation of organic dyes through selective adsorption enrichment by using a complex film of CdS and carboxylmethyl starch, J. Environ. Manage. 274 (2020) 3.

[46] T.D. Savic, M.V. Carevic, M.N. Mitric, J.Z. Kuljanin-Jakovljevic, N.D. Abazovic, M. I. Comor, Simulated solar light driven performance of nanosized $ZnIn_2S_4$/dye system: decolourization vs. photodegradation, J. Photochem. Photobiol. A-Chem. 388 (2020) 1.

[47] P. Li, X. Zhao, H.G. Sun, L. Wang, B. Song, B.Y. Gao, W.L. Fan, Theoretical studies on the form and effect of N-doping in an $ZnGa_2O_4$ photocatalyst, RSC Adv. 6 (2016) 74483–74492.

[48] T. Tachikawa, M. Fujitsuka, T. Majima, Mechanistic insight into the TiO_2 photocatalytic reactions: design of new photocatalysts, J. Phys. Chem. C 111 (2007) 5259–5275.
[49] M.A. Mahadik, G.W. An, S. David, S.H. Choi, M. Cho, J.S. Jang, Fabrication of A/R-TiO_2 composite for enhanced photoelectrochemical performance: solar hydrogen generation and dye degradation, Appl. Surf. Sci. 426 (2017) 833–843.
[50] Y. Nosaka, A.Y. Nosaka, Generation and detection of reactive oxygen species in photocatalysis, Chem. Rev. 117 (2017) 11302–11336.